JETIR.ORG ISSN: 2349-5162 | ESTD Year : 2014 | Monthly Issue
JOURNAL OF EMERGING TECHNOLOGIES AND INNOVATIVE RESEARCH (JETIR)
An International Scholarly Open Access, Peer-reviewed, Refereed Journal

Study of Refractive Index Profile near the Surface of YVO_4 Waveguide using Point Dipole Approach

[1]A. Rajasri, [2]G. S. Kumar, [3]P. Manoher
[1]Assistant Professor, [2]Former Professor, [3]Assitant Professor (C)
[1]Department of Physics,
[1]Pingle Government College for Women, Warangal, Telangana, India

Abstract : Yttrium Ortho Vanadate (YVO_4) is a positive uniaxial, wide transparency range optical fiber material with large birefringence. The variation of refractive indices near the surface of YVO_4 optical fibers is observed. The "Local" fields experienced by ions near the surface of fiber material are different from those in the interior. Using theoretical Point Dipole Approximation (PDA), one can calculate refractive index variation near the surface of the material. In thin films and optical waveguides, this variation can alter the propagation characteristics. The variation of ordinary and extraordinary refractive indices n_o and n_e from the surface to a depth of 71.2Å near the surface for Z-cut and *X*-cut YVO_4 waveguides are evaluated using PDA. For a *Z*-cut waveguide, n_o is found to increase from surface to the interior whereas n_e is found to decrease from surface to the interior. For an *X*-cut, Z-propagation waveguide, n_o is found to decrease from the surface to the interior whereas, n_e is found to increase from the surface to the interior. It is observed that the refractive indices n_o, and n_e variation and also the birefringence (dn= n_e -n_o) variation with depth near the surface for both the cases are quite opposite in nature.

IndexTerms **- Point Diople Approximation, refractive index, birefriengence, YVO_4 waveguide, thin film.**

I. INTRODUCTION

Extensive research work has been carried out on rare earth Orthovanadate, as it is significant oxide in material science and technology (Baogeng Xie, 2020, Chinh, 2019 and Naveen, 2018). Particularly, Yttrium Orthovanadate (YVO_4) has immense applications in fields such as laser host material (Banal, 2014 and Huang, 2011) and polarizer (Chen, 2006 and Lagatsky, 2005). Because of its large birefringence (Δn =0.2225 at 6328Å), it has high damage threshold, high conductivity, good mechanical properties and chemical stability (Shuai Wang ,2021, Huang, 2012 and Milev, 2007). It is also widely used as optical isolator and beam displacer (Tang, 2007 and Wang, 2009).The compound attracted many researchers for its large birefringence, non-linear coefficients, and effectively no infrared absorption from 2.5 to 15mm (Mey, 2012 and Messekine, 2010). It can be considered as the oldest laser host crystal for Nd^{+3} ions (Kaminskii, 1969 and O'Conner, 1966) and EU^{+3}:YVO_4 acts as highly efficient red emitting phosphor. In the characterization of optical devices the Refractive Index is an important parameter and understanding of this from atomic point of view is very essential. Present day interest in every field is to assess the behavior of the sample at nano-scale. Hence the proposed work is aimed at calculating the Refractive Indices values at atomic level.

II. EXPRESSIONS FOR REFRACTIVE INDICES – A POINT DIPOLE APPROACH

In the Point Dipole Approach (PDA) method, the ions in YVO_4 waveguide are polarizable points that can accurately approximate the response of a continuum target in the bulk. Each ion can be treated as a point dipole oscillating under the electric field of the incident e.m. radiation. The sum of external field and the field due to all the oscillating dipoles around the ion represents the total field acting on each ion. The Clausius-Mossotti relation, eqn.(1)-eqn.(3), helps us to evaluate the electronic polarizabilities of ions at a given wavelength say 6328Å by using the refractive indices values from the experimental data (DeShazer, 1987).

$$\chi_x = \frac{P_x}{E_x} = \frac{\varepsilon_x - 1}{4\pi} = \frac{n_x^2 - 1}{4\pi} = \frac{\sum_j N_j \alpha_j [1 + \sum_i D_{ij} \alpha_i]}{1 - \sum_j N_j \alpha_j [1 + \sum_i D_{ij} \alpha_i] K_x} \quad (1)$$

$$\frac{n_y^2 - 1}{4\pi} = \frac{\sum_j N_j \alpha_j [1 + \sum_i D_{ij} \alpha_i]}{1 - \sum_j N_j \alpha_j [1 + \sum_i D_{ij} \alpha_i] K_y} \quad (2)$$

$$\frac{n_z^2 - 1}{4\pi} = \frac{\sum_j N_j \alpha_j [1 + \sum_i D_{ij} \alpha_i]}{1 - \sum_j N_j \alpha_j [1 + \sum_i D_{ij} \alpha_i] K_z} \qquad (3)$$

where $\sum_j \sum_i D_{X\,ij} = \sum_j \sum_i \frac{3x_i^2 - r_i^2}{r_i^5}$ is a measure of the lattice anisotropy factor or geometric anisotropy in the *X*-direction for all the i^{th} ions with j^{th} ion at the center and $K_x = K_y = K_z = 4\pi/3$ is the depolarization factor for spherical cavity.

From eqn. (1) to eqn. (3) one can evaluate, electronic polarizabilities of ions by using the lattice anisotropy factors summations for various ions in the core of the YVO_4 waveguide along the cartesian axes. The lattice anisotropy factors cartesian components are calculated at a depth of 10 times of lattice constant 'a=7.12Å' inside the core of YVO_4 waveguide and are shown in Table 2.

As Refractive Index is due to the dipole moments of the ions which can be expressed in terms of the effective local fields at the site of the ions and the polarizability of the ions. The ions on the surface and near the surface have a different effective local field as compared to the ions well within the medium. This is because an ion near the surface sees a different environment when compared to an ion well within the lattice. There will be, consequently a variation in electrical field from ion to ion is observed as we move from the surface to the interior of the waveguide. Thus the geometric anisotropy factors $\Sigma_j \Sigma_i D_{ij}$'s would also vary from the surface to the interior and a gradation of refractive index n_o or n_e from the surface to interior results.

Let us consider a YVO_4 waveguide placed in an external electric field E_0 of the incident light wave. Each atom of the waveguide becomes a dipole under the action of the electric field. Thus dipole moments could be attributed to these atoms and are treated as point dipoles at the appropriate lattice sites. The Lorentz fields are then evaluated at different lattice sites in the unit cell caused due to different atomic dipoles surrounding them by PDA method which is used so far by (Praveena, 1989, Ramesh, 1993, Ramesh, 1994, Manoher, 2015, Satyanarayan Reddy, 2016 and Suhasini, 2021).

III. CALCULATIONS

For the purpose of calculation, the *X*-cut and *Z*-cut waveguides are considered separately, with propagation directions coinciding with the normals to the faces cut. For an *X*-cut waveguide, the direction of propagation is chosen along *X* direction so that the electric vector of light oscillates in the *YZ* plane. For a *Y*-cut waveguide, the direction of propagation is chosen along *Y* direction so that the electric vector of light oscillates in the *XZ* plane. For a *Z*-cut waveguide, the direction of propagation is chosen along *Z* direction so that the electric vector of light oscillates in the *XY* plane. Table 1 lists various cuts of a given waveguide along with cartesian propagation directions to know n_o or n_e.

For YVO_4 waveguide which is uniaxial (a=b=7.12Å and c=6.289Å), only two cuts are possible i.e. *X*-cut and *Z*-cut. *Y*-cut is same as *X*-cut. Only one optic axis is observed i.e along crystallographic c-axis. If light propagates along c-axis, the electric vibration is uniform in the *XY* plane. So n_e is observed along crystallographic *c*-axis or Cartesian *Z*-axis.

An iterative programme is written in C++ to calculate n_x, n_y and n_z and by using equation (1), equation (2) and equation (3) for the electric vector vibrating along the *X* , *Y* and *Z* axes by varying the values of polarizabilities α_i in small increments, one at a time within the range of their practically observed values. The local anisotropic factors '$\Sigma_j \Sigma_i D_{ij}$'s' are calculated and given in Table 2 The polarizability values tuned to fit the calculated refractive indices with the experimental values (DeShazer, 1987) are shown in Table 3.

Table 1: n_o and n_e representations along cartesian axes for *X*, *Y* and *Z*-cut waveguides

Crystal Axis ‖ Cartesian Axis	n_x	n_y	n_z	Configuration Names
c-axis ‖ X-axis	n_e	n_o	n_o	*Y*-cut, *X*-propagation *Z*-cut, *X*-propagation
c-axis ‖ Y-axis	n_o	n_e	n_o	*X*-cut, *Y*-propagation *Z*-cut, *Y*-propagation
c-axis ‖ Z-axis	n_o	n_o	n_e	*X*-cut, *Z*-propagation *Y*-cut, Z-propagation

Table 2: Lattice Anisotropy Factors $\left(\sum_j \sum_i D_{X_{ij}} / \sum_j \sum_i D_{Z_{ij}} \right) \times 10^{-24} cm^3$ values obtained using PDA within the Core of YVO_4 Optical Waveguide at λ=6328Å along Cartesian *X* and *Z*-axes

Effect On → / Effect due to↓	$\sum_j \sum_i D_{X\,ij} = \sum_j \sum_i \frac{3x_i^2 - r_i^2}{r_i^5}$			$\sum_j \sum_i D_{Z\,ij} = \sum_j \sum_i \frac{3z_i^2 - r_i^2}{r_i^5}$		
	Y_j	V_j	O_j	Y_j	V_j	O_j
Y_i	0.042625	0.156712	0.016186	-0.085249	0.313424	0.032371
V_i	0.156712	0.042625	-0.344646	0.313424	-0.085249	0.689293
O_i	-0.016186	-0.344646	0.161745	0.032371	0.689293	0.323490

Table 3: Electronic polarizability tuned values for various constituent ions of *YVO_4* waveguide at λ=6328Å

Electronic Polarizability $\alpha \times 10^{-24}cm^3$	Refractive Indices			Birefringence ($\Delta n = n_e - n_o$)	
	n	Calculated	Experimental	Calculated	Experimental
α_Y= 0.55 α_V = 0.5515 α_O = 2.1998	$n_x = n_o$ $n_y = n_o$ $n_z = n_e$	1.9929 1.9929 2.2154	1.9929 1.9929 2.2154	0.2225	0.2225

I. VARIATION OF REFRACTIVE INDICES AND BIREFRINGENCE NEAR THE SURFACE OF A *Z*-CUT, *X*-PROPAGATION YVO_4 WAVEGUIDE

Here the cartesian *X-axis* of the unit cell coincides with the Z-axis of the waveguide (See Table-1). To calculate the variation of the Refractive Indices near the surface, the waveguide is divided into regions of one-unit cell dimensions normal to the surface. A unit cell of YVO_4 touching the surface of the waveguide is considered. This unit cell is represented as 0^{th} unit cell. The local field effects at the different lattice sites with this position of the sphere are evaluated. The centre is then shifted to 1^{st} unit cell below the surface and local fields are evaluated. This procedure is continued until the radius of the sphere of influence is 71.2Å which corresponds to 10 times the lattice constant '*a*'.

Table 4: Lattice Anisotropy Factors ($\sum_j \sum_i D_{X\,ij} / \sum_j \sum_i D_{Z\,ij}$) × $10^{-24}cm^3$ for *Z*-Cut, *X*-Propagation YVO_4 Waveguide at various Depths for λ=6328Å

Effect On → / Effect due to ↓	$\sum_j \sum_i D_{X\,ij} = \sum_j \sum_i \frac{3x_i^2 - r_i^2}{r_i^5}$			$\sum_j \sum_i D_{Z\,ij} = \sum_j \sum_i \frac{3z_i^2 - r_i^2}{r_i^5}$		
	Y_j	V_j	O_j	Y_j	V_j	O_j
0^{th} Unit Cell below the Surface (0Å – 7.12Å)						
Y_i	-0.149860	-0.356146	-0.753163	0.001911	0.416929	0.397351
V_i	-0.356146	-0.149860	-1.124412	0.416929	0.001911	1.088151
O_i	-0.838662	-1.217130	-2.961399	0.303985	0.912475	1.706319
1^{st} Unit Cell below the Surface (7.12Å – 14.24Å)						
Y_i	-0.120413	-0.319962	-0.653823	-0.003812	0.395080	0.351261
V_i	-0.319962	-0.120413	-0.982470	0.395080	-0.003812	1.008274
O_i	-0.684569	-1.013359	-2.773758	0.366561	1.023710	1.629409
2^{nd} Unit Cell below the Surface (14.24Å – 21.36Å)						
Y_i	-0.090152	-0.289728	-0.533610	-0.018923	0.379981	0.291116
V_i	-0.289728	-0.090152	-0.862147	0.379981	-0.018923	0.947998
O_i	-0.563134	-0.891686	-2.290427	0.305928	0.962831	1.387509
3^{rd} Unit Cell below the Surface (21.36Å – 28.48Å)						
Y_i	-0.061489	-0.261095	-0.419970	-0.033229	0.365641	0.234283
V_i	-0.261095	-0.061489	-0.748476	0.365641	-0.033229	0.891245
O_i	-0.447611	-0.776116	-1.832146	0.248088	0.905026	1.158343
4^{th} Unit Cell below the Surface (28.48Å – 35.60Å)						
Y_i	-0.035035	-0.234651	-0.315519	-0.046424	0.352350	0.182034
V_i	-0.234651	-0.035035	-0.644047	0.352350	-0.046424	0.839012
O_i	-0.340637	-0.669153	-1.409016	0.194594	0.851583	0.946919
5^{th} Unit Cell below the Surface (35.60Å – 42.72Å)						
Y_i	-0.011430	-0.211058	-0.222676	-0.058209	0.340580	0.135589
V_i	-0.211058	-0.011430	-0.551222	0.340580	-0.058209	0.792583
O_i	-0.244651	-0.573198	-1.031385	0.146591	0.803577	0.758232
6^{th} Unit Cell below the Surface (42.72Å – 49.84Å)						
Y_i	0.008711	-0.190918	-0.144046	-0.068283	0.330559	0.096218
V_i	-0.190918	0.008711	-0.472591	0.330559	-0.068283	0.753257
O_i	-0.162236	-0.490778	-0.709305	0.105306	0.762340	0.597197
7^{th} Unit Cell below the Surface (49.84Å – 56.96Å)						
Y_i	0.024735	-0.174848	-0.082097	-0.076290	0.322495	0.065327
V_i	-0.174848	0.024735	-0.410740	0.322495	-0.076290	0.722352
O_i	-0.095875	-0.424475	-0.452929	0.072197	0.729242	0.469107
8^{th} Unit Cell below the Surface (56.96Å – 64.08Å)						
Y_i	0.035988	-0.163532	-0.039315	-0.081927	0.316841	0.043935
V_i	-0.163532	0.035988	-0.368100	0.316841	-0.081927	0.701010
O_i	-0.048077	-0.376833	-0.272190	0.048320	0.705380	0.378715
9^{th} Unit Cell below the Surface (64.08Å – 71.20Å)						
Y_i	0.041857	-0.157515	-0.018422	-0.084863	0.313826	0.033489
V_i	-0.157515	0.041857	-0.346994	0.313826	-0.084863	0.690464
O_i	-0.021428	-0.350118	-0.177646	0.034989	0.692020	0.331458

10^{th} Unit Cell below the Surface (71.20Å – 78.32Å)						
Y_i	0.042625	-0.156712	-0.016186	-0.085249	0.313424	0.032371
V_i	-0.156712	0.042625	-0.344646	0.313424	-0.085249	0.689293
O_i	-0.016186	-0.344646	-0.161745	0.032371	0.689293	0.323490

The local anisotropic factors '$\Sigma_j\Sigma_i D_{ij}$'s are given in Table 4. The values given in these tables represent the 'local field' as seen by each of the species of Y, V and O *atoms*. The values of Refractive Indices and Birefringence are given in Table 5.

Table 5: n_o, n_e and Δn variation near the surface for *Z*-cut, *X*-propagation waveguide at λ=6328Å.

Depth (in Å)	Refractive Indices		Birefringence
	n_o	n_e	$(\Delta n = n_e - n_o)$
0 × a = 0	1.44352	2.68995	1.24643
1 × a = 7.12	1.48653	2.66718	1.18065
2 × a = 14.24	1.56618	2.56999	1.00382
3 × a = 21.36	1.64647	2.48444	0.83797
4 × a = 28.48	1.72540	2.41047	0.68507
5 × a = 35.60	1.80036	2.34802	0.54766
6 × a = 42.72	1.86814	2.29716	0.42902
7 × a = 49.84	1.92495	2.25819	0.33324
8 × a = 56.96	1.96667	2.23142	0.26474
9 × a = 64.08	1.98913	2.21763	0.22850
10 × a = 71.20	1.99290	2.21535	0.22245

*a = 7.12Å is the lattice constant along *a*-axis.

II. VARIATION OF REFRACTIVE INDICES AND BIREFRINGENCE NEAR THE SURFACE FOR AN X-CUT, Z-PROPAGATION YVO_4 WAVEGUIDE

In Table 1, n_o and n_e directions for various crystal cuts in various Cartesian propagation directions are listed. For an open type *X*-cut YVO_4 waveguide, with the light propagation direction along *Z*-axis the *c*-axis of the unit cell coincides with the *X*-axis of the waveguide. The electric vector of light is considered to be along *X* and *Z* directions leading to evaluation of n_e and n_o in the waveguide.

Table 6: Lattice Anisotropy Factors ($\sum_j \sum_i D_{X\,ij} / \sum_j \sum_i D_{Z\,ij}$) × 10^{-24}cm^3 for an *X*-Cut, *Z*-Propagation YVO_4 Waveguide for Various Depths at λ=6328Å.

Effect On → Effect due to↓	$\sum_j \sum_i D_{X\,ij} = \sum_j \sum_i \frac{3x_i^2 - r_i^2}{r_i^5}$			$\sum_j \sum_i D_{Z\,ij} = \sum_j \sum_i \frac{3z_i^2 - r_i^2}{r_i^5}$		
	Y_j	V_j	O_j	Y_j	V_j	O_j
0^{th} Unit Cell below the Surface (0Å – 6.289Å)						
Y_i	0.144196	-0.068155	0.445151	-0.218486	0.066405	-0.728737
V_i	-0.068155	0.144196	-0.327417	0.066405	-0.218486	-0.071507
O_i	0.445151	-0.327417	1.216041	-0.728737	-0.071507	-2.436921
1^{st} Unit Cell below the Surface (6.289Å – 12.578Å)						
Y_i	0.127201	-0.072475	0.321114	-0.254003	0.144552	-0.641710
V_i	-0.072475	0.127201	-0.007304	0.144552	-0.254003	0.014110
O_i	0.321114	-0.007304	1.188470	-0.641710	0.014110	-2.375668
2^{nd} Unit Cell below the Surface (12.578Å – 18.867Å)						
Y_i	0.113598	-0.085835	0.267304	-0.227176	0.171650	-0.534661
V_i	-0.085835	0.113598	-0.061255	0.171650	-0.227176	0.122523
O_i	0.267304	-0.061255	0.972587	-0.534661	0.122523	-1.945298
3^{rd} Unit Cell below the Surface (18.867Å - 25.156Å)						
Y_i	0.100670	-0.098738	0.215602	-0.201299	0.197434	-0.431190
V_i	-0.098738	0.100670	-0.112945	0.197434	-0.201299	0.225861
O_i	0.215602	-0.112945	0.765848	0.431190	0.225861	-1.531488
4^{th} Unit Cell below the Surface (25.156Å – 31.445Å)						
Y_i	0.088434	-0.110854	0.166970	-0.176910	0.221749	-0.333867
V_i	-0.110854	0.088434	-0.161610	0.221749	-0.176910	0.323209
O_i	0.166970	-0.161610	0.570886	-0.333867	0.323209	-1.141730
5^{th} Unit Cell below the Surface (31.445Å – 37.734Å)						
Y_i	0.077251	-0.122063	0.122194	-0.154493	0.244118	-0.244329
V_i	-0.122063	0.077251	-0.206381	0.244118	-0.154493	0.412749
O_i	0.122194	-0.206381	0.391757	-0.244329	0.412749	-0.783477
6^{th} Unit Cell below the Surface (37.734Å – 44.023Å)						

Y_i	0.067240	-0.132057	0.082152	-0.134490	0.264125	-0.164361
V_i	-0.132057	0.067240	-0.246347	0.264125	-0.134490	0.492745
O_i	0.082152	-0.246347	0.231760	-0.164361	0.492745	-0.463557
7th Unit Cell below the Surface (44.023Å – 50.312Å)						
Y_i	0.058672	-0.140657	0.047856	-0.117326	0.281296	-0.095682
V_i	-0.140657	0.058672	-0.280725	0.281296	-0.117326	0.561426
O_i	0.047856	-0.280725	0.094479	-0.095682	0.561426	-0.188918
8th Unit Cell below the Surface (50.312Å – 56.601Å)						
Y_i	0.051703	-0.147623	0.020021	-0.103380	0.295219	-0.040030
V_i	-0.147623	0.051703	-0.308565	0.295219	-0.103380	0.617081
O_i	0.020021	-0.308565	-0.016919	-0.040030	0.617081	0.033815
9th Unit Cell below the Surface (56.601Å - 62.89Å)						
Y_i	0.046599	-0.152763	-0.000370	-0.093196	0.305523	0.000757
V_i	-0.152763	0.046599	-0.328967	0.305523	-0.093196	0.657928
O_i	-0.000370	-0.328967	-0.098531	0.000757	0.657928	0.197027
10th Unit Cell below the Surface (62.89Å - 69.179Å)						
Y_i	0.043570	-0.155813	-0.012562	-0.087140	0.311626	0.025118
V_i	-0.155813	0.043570	-0.341129	0.311626	-0.087140	0.682255
O_i	-0.012562	-0.341129	-0.147078	0.025118	0.682255	0.294183
11th Unit Cell below the Surface (69.315Å – 83.178Å)						
Y_i	0.042641	-0.156696	-0.016141	-0.085282	0.313391	0.032283
V_i	-0.156696	0.042641	-0.344597	0.313391	-0.085282	0.689194
O_i	-0.016141	-0.344597	-0.161523	0.032283	0.689194	0.323046

In order to calculate the variation of the Refractive Indices near the surface, the waveguide is divided into regions of one-unit cell dimensions normal to the surface. As the Z-axis of the unit cell coincides with the *X*-axis of the waveguide. The 0th unit cell covers up to a depth of *c*=6.289Å, 1st unit cell depth is of 2*c*, 2nd unit cell depth is of 3*c*, 3rd unit cell depth is of 4c and so on and 10th unit cell depth is of 11c below the surface, which covers the core radius or depth.

Table 7: n_o, n_e and Δn variation near the surface for *X*-cut, *Z*-propagation YVO_4 waveguide at λ=6328Å.

Depth (in Å)	Refractive Indices		Birefringence
	n_o	n_e	$(\Delta n = n_e - n_o)$
0 × c = 0	2.35305	1.5927	-0.76035
1 × c = 6.289	2.37063	1.6138	-0.75683
2 × c = 12.578	2.30172	1.6921	-0.60962
3 × c = 18.867	2.29459	1.7007	-0.59389
4 × c = 25.156	2.23282	1.7809	-0.45192
5 × c = 31.445	2.17748	1.8613	-0.31618
6 × c = 37.734	2.09128	2.0071	-0.08418
7 × c = 44.023	2.05603	2.0758	0.01977
8 × c = 50.312	2.02817	2.1345	0.10633
9 × c = 56.601	2.00816	2.1794	0.17124
10 × c = 62.890	1.99290	2.2154	0.22250
11 × c = 69.179	1.99290	2.2154	0.22250
10 × a = 71.200	1.99290	2.2154	0.22250

*a = 7.12Å is the lattice constant along *a*-axis.
*c = 6.289Å is the lattice constant along *a*-axis.

To calculate the refractive indices on the surface, a unit cell of YVO_4 touching the surface of the waveguide is considered. This unit cell is represented as 0th unit cell. The Local field effects are within a radius of 6.289*A*º for different lattice sites with this position are evaluated. The centre is then shifted to 1st unit cell below the surface and local fields are evaluated. This procedure is continued to to ten times the lattice constant 'c' where the radius of the sphere of influence is 62.89Å. At this position all the sphere of local field is totally within the core of the waveguide.

The local anisotropic factors '$\Sigma_j \Sigma_i D_{ij}$'s' are given in Table 6. The values given in these tables represent the 'local field' as seen by each of the species of Y, V and O *atoms*. The values of Refractive Indices and Birefringence are given in Table 7.

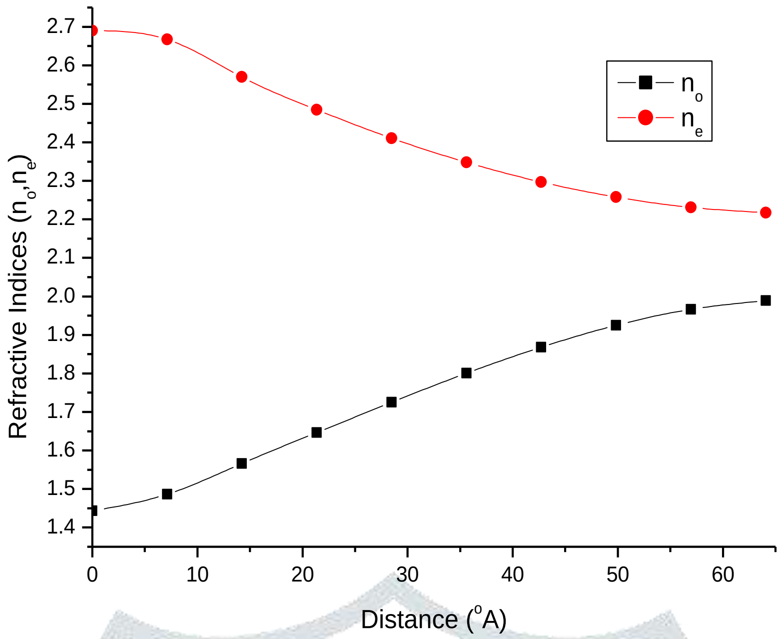

Figure 1: Variation of n_o and n_e near the Surface of an *Z*-cut, *X*-propagation YVO_4 Waveguide at λ = 6328Å.

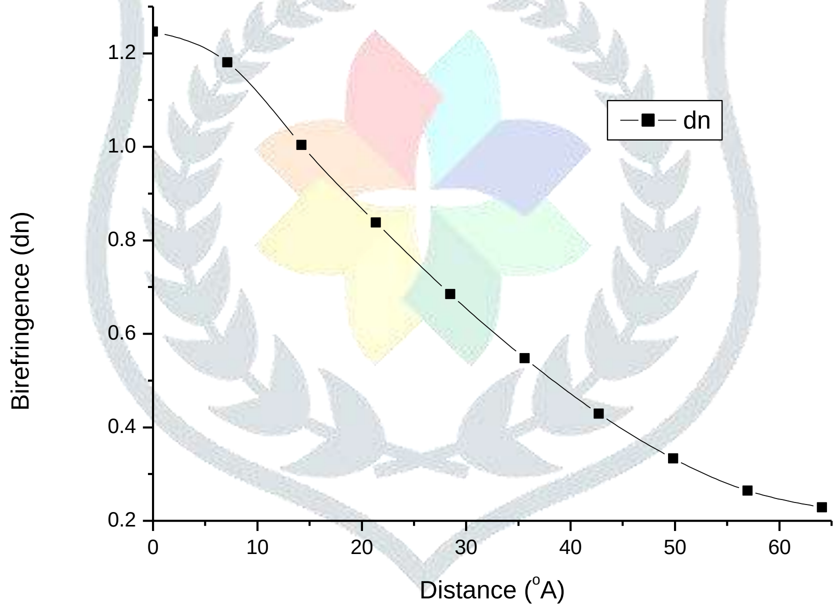

Figure 2: Variation of Birefringence near the Surface of an *Z*-cut, *X*-propagation YVO_4 Waveguide at λ = 6328Å.

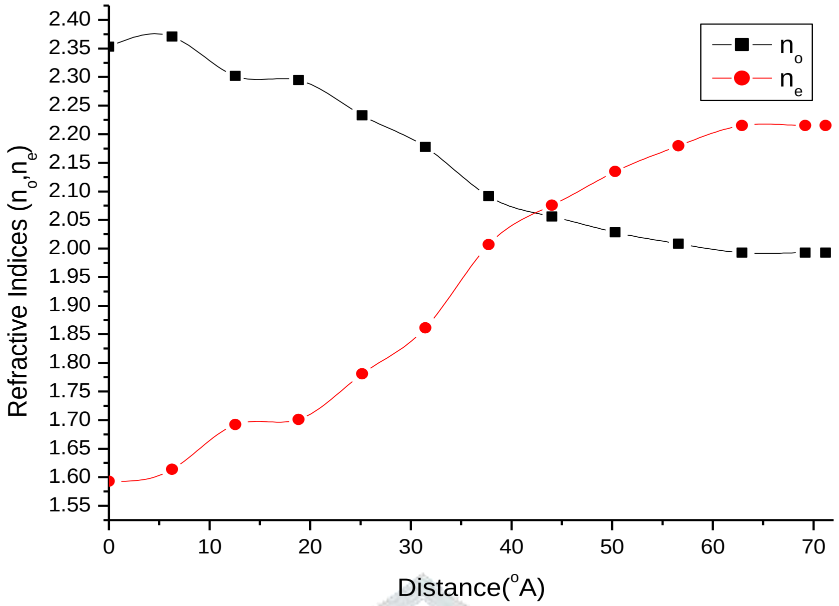

Figure 3. Variation of n_o and n_e near the Surface of a *X*-cut, *Z*-propagation YVO_4 Waveguide at λ = 6328Å.

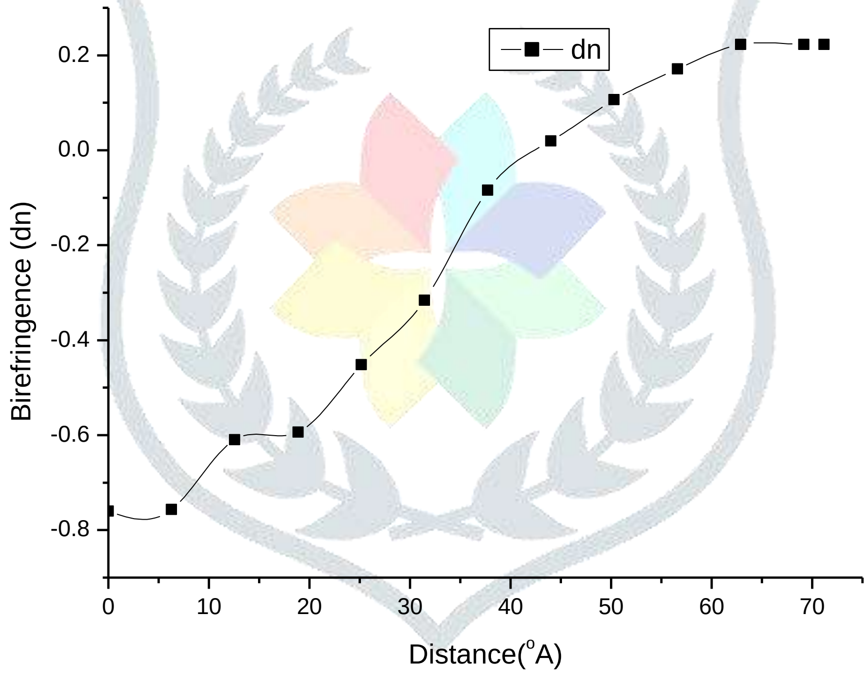

Figure 4. Variation of Birefringence near the Surface of a *X*-cut, *Z*-propagation YVO_4 Waveguide at λ = 6328Å.

VI. RESULTS AND DISCUSSION

The calculations are carried out for YVO_4 optical waveguide at wavelength 6328Å. For an *X*-cut, Z-propagation YVO_4 waveguide, n_o is found to increase from 1.44 on the surface to 1.99 in the interior, whereas n_e is found to decrease from 2.69 on the surface to 2.22 in the interior of the waveguide. For a *Z*-cut waveguide, n_o is found to increase from 1.44 to 1.99 whereas n_e is found to decrease from 2.69 to 2.22. The opposite behavior in the variation of *no* and *ne* near the surface of the *X*–cut, and *Z*–cut waveguides are primarily due to the dipole orientation in the lattice being different for the two directions of the electric vectors of light.

Variation of the refractive index near the surface is to be considered in the studies involving the propagation mechanisms of light through all such waveguides.

REFERENCES

[1] Baogeng Xie, Min Chen, Junyue Lin, Xiaobing Liu, Shujun Peng, and Luping Zhong. 2020. Simple Methods to Synthesize YVO_4 Nanocrystals or Microcrystals without Any Templates or Surfactants. Journal of Chemistry, Vol. 2020, Article ID 3878409, 7 pages.

[2] Chinh DT, Phuong TPH, Thi MDD, and Chien MD. 2019. Sonochemical synthesis and properties of YVO_4: Eu^{3+}nanocrystals for luminescent security ink applications. Journal of Chemistry, vol. 2019, Article ID 5749702, 13 pages.

[3] Naveen KV, Neerugatti KE, Satyapaul, AS, and Giridhar M. 2018. Cocatalyst free Z-schematic enhanced H2 evolution over LaVO4/BiVO4 composite photocatalyst using Ag as an electron mediator. Appllied Catalysis B: Environmental, vol. 220, pp. 512–523.

[4] Banal RG, Taniyasu Y, and Yamamoto H. 2014. Deep-ultraviolet light emission properties of nonpolar M-plane AlGaN quantum wells. Appllied Physics Letters, vol. 105, no. 5, Article ID 053104.

[5] Huang JH, Deng J, Cao YG, *et al*. 2011. Passively mode-locked radially polarized laser based on ceramic Nd:YAG rod. OpticsExpress, vol. 19, pp. 2120–2124.

[6] Chen L, Liu Y, and Huang K. 2006. Hydrothermal synthesis and characterization of YVO_4-based phosphors doped with Eu^{3+} ion. Materials Research Bulletin, vol. 41, no. 1, pp. 158–166.

[7] Lagatsky AA, Sarmani AR, Brown CTA *et al*. 2005. Yb^{3+} doped YVO_4 crystal for efficient Kerr-lens mode locking in solid-state lasers. Optics Letters, vol. 30, no. 23, pp. 3234– 3239.

[8] Shuai Wang, Pengfei Wang, Yongfeng Ruan, Youfa Wang, and Shouchao Zhang. 2021. Photoluminescence characteristics and energy transfer phenomena in Ce3+-doped YVO_4 single Crystal. Science and Engineering of Composite Materials. 28: 205–214.

[9] Huang ZC, Feng J, Pan W. 2012. Theoretical investigations of the physical properties of zircon-type YVO_4. J Solid State Chem.185:42–8.

[10] Milev DR, Atanasov PA, Dikovska AO, Dimitrov IG, Petrov KP, Avdeev. 2007. GV. Structural and optical properties of YVO_4 thin films. Appl Surf Sci. 253:8250–3.

[11] Tang XD, Ding ZJ, Zhang ZM, Lumin J. 2007. Membrane fluidity altering and enzyme inactivating in sarcoma 180 cells post the exposure to sonoactivated hematoporphyrin in vitro.Ultrasonics. 122:66–73.

[12] Wang Y, Qin WP, Zhang JS, Cao CY, Lü SZ, Ren XG. 2009. Photoluminescence of colloidal YVO_4:Eu/SiO2 core/shell nanocrystals. Opt Commun. 282:1148–53.

[13] Mei Y, Zheng WC, Yang YG, Liu HG. 2012. An interpretation of the g factors for the tetragonally-compressed Cr^{5+} centers in YVO_4 and YPO_4 crystals. Phys B. 407:4365.

[14] Messekine Souad, Sahnoun Mohammed, Driz Mohamed and Daul Claude. 2010. The effect of pressure on the structural and electronic properties of yttrium orthovanadate YVO_4 compound: total-energy calculations. Z. Kristallogr. 225; 514–519.

[15] Kaminskii AA, Bogomolova GA and Li L.1969 .Absorption, fluorescence, stimulated emission and splitting of the Nd3þ levels in a YVO_4 crystal. Inorg. Mater. (USSR) 5; 573.

[16] O'Conner JR. 1966. Unusual crystal-field energy levels and efficient laser properties of YVO_4:Nd. Appl. Phys. Lett. 9; 407.

[17] DeShazer LG, Rand SC, Wechsler BA. 1987. Handbook of Laser Science and Technology, Vol. V: Optical materials part 3. Boca Raton, Florida: CRC Press. p. 283. ISBN 0-8493-3505-1.

[18] Praveena D, Siddiqui MAA, Kumar GS and Ethiraj R. 1989. Electronic polarizabilities of ions in KDP and ADP from natural birefringence data. J Materials Science Letters, 8(4): 496.

[19] Ramesh N. and Ethiraj R. 1993. Variation of Refractive Index n_o near the surface of LiNbO3 Open type Wave guide. IEEE/LEOS Proc, Conference OPTCON' 93, California.

[20] Ramesh N and Ethiraj R. 1994. Electronic polarizabilities of ions in lithium niobate crystal. J Materials Science Letters, 13(10): 757-758.

[21] Manoher P. Sathyanarayan Reddy B. and Ethiraj R. 2015. Study of Thermo–Polarizability of Ions in Lithium Rich LiNbO3 by the Point Dipole Approximation. IJTT, 5(4):306-310.

[22] Sathyanarayan Reddy B, Manoher P, Ethiraj R and Gopal Reddy Ch. 2016. Thermo Optic and Thermo Polarizability Coefficients of Lithium Rich LiNbO3 by the Point Dipole Approximation. IJCET, 6(1):112-116.

[23] Suhasini V, Subbareddy IV, Manoher P, Srinivasa Rao V, and Ethiraj R. 2021. Study of Refractive Index and Birefringence Variation near the Surface of LiNbO3 Open Type Optical Waveguide using Point Dipole Approximation. J. Phys.: Conf. Ser. 1817 012024.